mater.scichina.com link.springer.com

Published online 15 April 2020 | https://doi.org/10.1007/s40843-020-1288-6
Sci China Mater 2020, 63(8): 1364–1381

SPECIAL ISSUE: Optical Gain Materials towards Enhanced Light-Matter Interactions

Optical property and lasing of GaAs-based nanowires

Haolin Li[1,2†], Yuting Chen[2†], Zhipeng Wei[1*] and Rui Chen[2*]

ABSTRACT GaAs-based nanowire (NW) lasers working in the infrared region is critical in integrated optoelectronics. In the past few decades, the field of NW lasers has developed rapidly. Compared with materials working in the ultraviolet and visible ranges, GaAs-based infrared NW lasers, however, are more difficult to achieve because of their specific properties. In this review, we focus on the recent developments of GaAs-based NWs, more especially, the optical property and lasing of GaAs-based NWs. The growth mechanism of GaAs NWs is introduced in detail, including the crystal phase control and the growth of complex structures. Subsequently, the influence and improvement of the optical properties of GaAs-based NWs are introduced and discussed. Finally, the design and latest progress of GaAs-based NW lasers are put forward.

Keywords: GaAs-based nanowires, quantum well, infrared, optical property, lasing

INTRODUCTION

With the development of artificial intelligence technology and the advent of the era of big data, humanity's demand for information is growing. Conventional information technologies are currently reaching their limits due to high latency and huge power consumption. Photons with faster transmission speeds and stronger anti-interference abilities will become the ideal information carrier for next-generation technology. The development of a photonic integrated circuit (PIC) will lead to the revolution of information technology [1]. As one of the most important devices in PIC, lasers have been widely investigated [2], especially for the GaAs-based lasers working at communication wavelengths [3]. The main focus of current laser research is their miniaturization and silicon-based integration to satisfy PIC development. Thanks to the quantum confinement effect, one-dimensional (1D) semiconductor nanowires (NWs) possess promising electronic and optical properties. High-quality NWs have a naturally smooth reflective surface that does not require further grinding and polishing. Their unique structure and high refractive index facilitate the propagation of photons inside the NWs to realize the light resonance, for example, the Fabry-Pérot (F-P) cavity defined by the NW end facets. Most importantly, due to non-planar 1D growth, the defects caused by lattice mismatches do not extend into the NW body, so the selectivity of NW growth to the substrate is not limited by the lattice mismatch. In other words, NWs show great advantages in silicon-based integration.

In 2001, the first demonstration of NW lasing was realized by using ZnO NWs [4], which opened a new era of NW lasers. The whole new field of NW lasers attracted attention from various research communities. NW laser materials have sprung up, including metal oxides, II-VI, and III-V semiconductor alloys, which cover the lasing wavelength from 370 to 2200 nm. Semiconductor materials with large bandgaps can be used in ultraviolet (UV) range, such as ZnO [4] and GaN [5]. Due to the large exciton binding energy and high optical gain, they do not need a long cavity to realize lasing. The first NW laser, therefore, was made of ZnO material. For lasers working in the visible range, the representative materials are CdS [6] and ZnSe [7], which show a great application in the field of lighting, imaging, and display. Infrared NW laser materials working in the communication range include GaAs [8–10], GaSb [11], and InP [12]. Among these reported infrared laser materials, GaAs has been widely considered because of its preparation convenience, direct bandgap, high gain value, and excellent bandgap tunability by changing the composition of GaAs-based alloys. The development of infrared lasing, however, is much

[1] State Key Laboratory of High Power Semiconductor Laser, School of Science, Changchun University of Science and Technology, Changchun 130022, China
[2] Department of Electrical and Electronic Engineering, Southern University of Science and Technology, Shenzhen 518055, China
[†] These authors contributed equally to this work.
[*] Corresponding authors (emails: chenr@sustech.edu.cn (Chen R); zpweicust@126.com (Wei Z))

more challenging compared with UV and visible NW lasers. As shown in the normalized modal dispersion relationship [13], NW lasers working in the infrared wavelength should be larger for effective waveguiding. Moreover, there will be more nonradiative recombination centers in narrow bandgap materials such as surface states and serious Auger recombination [8,10,11]. Last, the exciton binding energy of a narrow bandgap semiconductor is, in general, small. For example, GaAs has an exciton binding energy of only around 5 meV, which is much smaller than the thermal energy at room temperature (25 meV at 300 K). Efficient radiative recombination in GaAs-based materials, therefore, requires excellent crystal quality, high emission efficiency, and efficient structural design.

In the past few decades, tremendous amount of progresses have been made in the field of GaAs-based NW lasing. The growth mechanism of GaAs NWs has been investigated, and GaAs NWs with excellent crystal quality have been obtained. The optical properties of GaAs NWs have been extensively studied. Many methods toward optical property improvement have been proposed, and optical pumped lasing at room temperature has been realized [8,9]. Complex NW structures have emerged, and the regulation of laser properties of NWs has greatly developed. In this review, we focus on the recent developments of GaAs-based NWs, especially, the optical property and lasing of GaAs-based NWs. We begin with reviewing the advances in growth and a basic understanding of GaAs-based NW growth mechanisms. In particular, the vapor-liquid-solid (VLS) mechanism makes it possible to grow and regulate NWs with complex structures, such as coaxial quantum well (QW) NWs and dot-in-rod NWs. Then the optical properties of GaAs-based NWs are discussed, including methods which can improve the optical gain of the materials, such as doping and passivation. We subsequently discuss various structural designs for NW lasers. Finally, challenges and outlooks toward high-performance GaAs-based NW lasers have been provided. Other fundamentals can be found in some previous good reviews [1,14–26].

GaAs-BASED NW GROWTH

To achieve lasing from GaAs-based NWs, high crystal quality and complex structures are of great significance. In the past decades, researchers started to gradually understand the growth mechanism of 1D NWs, and NWs with a new structure were designed and fabricated. Growing GaAs-based NWs with well-defined crystal structures is a challenging task, but critical for device applications. This section will focus on the growth of NWs. We will briefly explain the growth mechanism and morphology control. We also discuss the phase control of NWs, the growth of doped NWs, and the complex QW structure of NWs [21,27–29].

GaAs NW growth and crystal phase control

Over the past few decades, the overall strategy for achieving GaAs-based NWs has not changed significantly. As for atomic-level epitaxy, metal-organic vapor phase epitaxy, and molecular beam epitaxy technologies are the main methods to grow GaAs NWs. Among them, the VLS growth mechanism was considered as the main method to grow the 1D semiconductor NWs [22] and was proposed by Wagner and Ellis [30] during the growth of Si whiskers in 1964. The VLS NW growth contains three distinct steps: alloying, nucleation, and growth. For GaAs-based NWs, the first step is the formation of catalyst droplets on a substrate. A certain proportion of the growth source gases then are passed into the growth chamber. Under appropriate growth temperature, gases nucleate in droplets and precipitate crystals along the growth direction to form NWs, as shown in Fig. 1a. Three conditions during the VLS growth show a significant influence on the properties of NWs: the catalyst, the source ratio, and temperature. Interestingly, Rudolph *et al.* [31] realized a droplet-free growth of GaAs NWs in a group V elements rich environment. But in this non-VLS growth mode, the NWs have a slow vertical growth rate. The catalyst is usually formed by droplets of Au or group III elements [32]. The pseudo-binary phase diagram of Au-GaAs shows that Au-GaAs liquid and GaAs solid are the principle phases above 630°C in the GaAs rich region. That is, Au could serve as a VLS catalyst in this region, according to the phase diagram [33]. Like every coin has two sides, using the Au catalyst will affect the optical properties of NWs. For example, NWs grown by an Au catalyst will form an Au particle on the top termination surface. Thanks to the ultralow refractive index of Au, it can achieve efficient end-face reflection, which is beneficial for light confinement [8]. Some researchers, however, found that the incorporation of Au during the VLS NW growth might be responsible for the limited performance of NW-based devices. Breuer and co-workers [34] compared the optical properties of gold-catalyzed and self-catalyzed GaAs NWs by time-resolved photoluminescence (TRPL) and temperature-dependent PL spectroscopy. The experimental results show that the PL lifetime of self-catalytic NWs is longer (~2.5 ns) while that of the Au-catalyzed NWs is

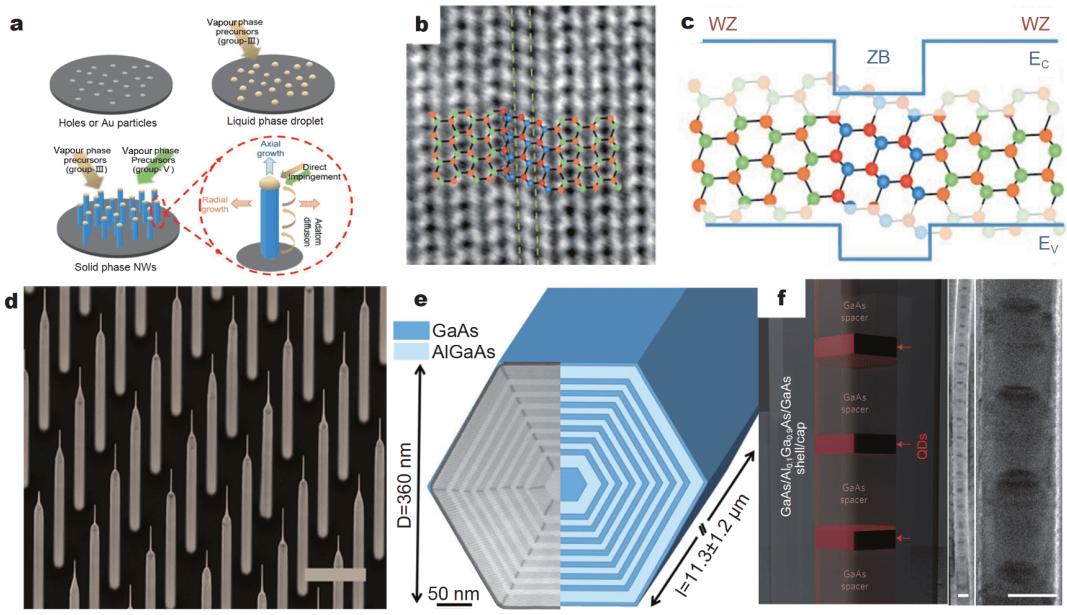

Figure 1 GaAs-based NW growth. (a) Scheme of the VLS growth mechanism. (b) HRTEM image of WZ/ZB mixed phase structure. (c) Atomic arrangement and band gap of WZ/ZB structure in same GaAs NWs. Reproduced with permission from [35]. Copyright 2009, American Physical Society. (d) Probe-like GaAs NWs formed by controlling droplet (scale bar: 1 μm). Reproduced with permission from [47]. Copyright 2017, American Chemical Society. (e) Coaxial GaAs/AlGaAs core-multi-shell QW NW. Reproduced with permission from [65]. Copyright 2016, AIP Publishing. (f) Dot-in-rod AlGaAs/GaAs axial QW NW (scale bars: 50 nm). Reproduced with permission from [88]. Copyright 2015, Springer Nature.

~9 ps, and the temperature stability of the material is better. Moreover, Au-catalyzed NWs do not adapt to Si-based integration.

When GaAs-based semiconductor materials are epitaxially grown in the form of NWs, metastable wurtzite (WZ) phases usually exist, while GaAs-based thin-film materials, in general, only exist in the stable zinc-blende (ZB) phase. Fig. 1b and c show the high-resolution transmission electron microscopy (HRTEM) images of the mixed phases in the NWs and the arrangement of the atoms [35]. Up to now, the growth of pure-phase GaAs-based NWs is still challenging. Nucleation at the triple-phase line (TPL) is used to address the experimentally observed formation of the WZ phase, as proposed by Glas *et al.* [36]. A nucleation-based model was proposed to describe the surface energy and formation energy. As is shown in this study, the higher cohesive energy of the WZ phase could be compensated by the lower surface energy during nucleation at the TPL.

Since then, the nucleation theory of NW growth has been further developed to include additional features such as the changes of the particle surface area [37], Kashchiev renormalization [38], poly-nucleation [39], droplet morphology [40,41], and droplet depletion [42]. Recently, Mårtensson and co-workers [43] presented a model to simulate the growth and crystal structure of GaAs NW, and their results match the experimental data. According to these theories, the flow of the group V precursor can control the crystal structure. In general, a high flow of an As precursor leads to the growth of the ZB phase, while lowering the As flow leads to WZ formation [44]. In 2010, Joyce *et al.* [45] demonstrated the phase-perfect Au-catalyzed NWs by tailoring the temperature and group V:III ratio. Meanwhile, Krogstrup's group grew Au-free GaAs NWs in the ZB phase by controlling the temperature and V:III ratio [46]. Kim and co-workers [47] grew nanoneedles in the pure WZ phase on top of NWs by controlling the V:III ratio and proved that the formation of WZ phase nanoneedles is related to the droplet contact angle. In 2019, Maliakkal and co-workers [48] used an *in situ* electron microscope and X-ray energy dispersive spectroscopy to measure the catalyst composition during NW growth. They studied the growth of Au-seeded GaAs NWs and found that the Ga content in the catalyst during growth increased with both temperature and Ga precursor flux. In the same year, the team of Schroth reported the impact of the shadowing effect on the crystal structure of patterned self-catalyzed GaAs NWs by using the simultaneous *in situ* X-ray investigation [49]. Their results indicated that the effective V:III

ratio could be adjusted by controlling the shadow effect brought by the spacing of NWs, thereby achieving effective phase control of NWs. Furthermore, phase control can also be performed by growing heterostructures and taking advantage of the strain induced by the lattice mismatch between different materials [50,51]. Moreover, the growth of pure-phase nanowires can also be achieved by doping, which will be discussed in the subsequent doping section.

The diameter and length of the NWs are related to the growth time, the growth temperature, and the V:III ratio. During the growth of NWs, the reactants involved in the growth originate from the direct impact and thermal migration along the sidewall, as indicated in Fig. 1a. Reaction species that impinge directly on the droplet contribute to the axial growth. Moreover, Ga adatoms adsorbed on the substrate and sidewalls will diffuse along the concentration gradient toward the droplet. These diffusing adatoms contribute to both radial and axial growths, and therefore, there is a competition between axial VLS growth and sidewall vapor-solid growth. At a lower temperature, the diffusing adatoms are less likely to be incorporated into NW sidewalls to limit the radial growth. Furthermore, the diffusion length of adatoms decreases with decreasing growth temperature [52]. This also explains the formation of probe-like NWs [47], as shown in Fig 1d.

Doping in GaAs NWs

Doping in GaAs NWs was first studied three decades ago [53], and research in this field has expanded rapidly in recent years. The main part of doping studies currently exists for Au or Ga seeded GaAs NWs [54–59]. The most commonly used n-type dopants are Te [55,57,60] and Si [61–63], while the most commonly used p-type dopants are Be [55,58,59,64], C [61], and Zn [54,56,57]. During the doped NW growth, the decomposition and diffusion of different growth species in the vapor phase on the surface of the NW and in the catalytic particles will affect the homogeneity of carrier concentration, material composition, and doping profile abruptness. Interestingly, it has been found that Be could be preferentially incorporated into certain facets underneath the seed particle during the NW growth [59]. This property can also be used for the crystal phase control of GaAs NWs. Be atoms accumulate inside the Ga droplets, leading to the change of the Ga droplet properties and causing the growth of pure-phase ZB NWs [58]. Due to the differences in incorporation paths for lateral and axial growths, the doping of NWs is usually accompanied by uneven or insufficient doping and crystal structure defects. An interesting approach to achieve doping while maintaining a high material quality is to employ modulation-doped core-shell structures [60–62]. The core-shell p-n junction allows the realization of electrically pumped lasers.

GaAs-based QW NW growth

In general, as the size decreases, NWs will exhibit better strain tolerance than bulk materials. Strain caused by lattice mismatch in the QW structure, therefore, can be better released. Due to the 1D structure of NWs, QW in NWs can be constructed in two ways, namely, the core-shell structure that forms a QW in the radial direction (Fig. 1e) [65–79], and the dot-in-rod structure that forms a QW in the axial direction (Fig. 1f) [80–88]. The difference between the axial and radial growths of QW NWs is the depletion of the droplets.

The method of radial QW NW growth is similar to the growth of core-shell NWs. The shell starts to grow immediately when the growth of the core is completed. During the growth of the shell, the axial growth of the NWs must be suppressed by controlling the temperature and equivalent beam ratio [78]. The growth time can obtain the axial QW NWs with different well thicknesses. When growing GaAs/GaAsSb QW NWs, we found that droplets can also control the morphology of core-shell NWs. If the Ga-catalyzed droplets on the top of the NWs are not completely consumed before the GaAsSb shell grows, a probe-like core-shell NW will appear [75]. This is related to the competition between the axial and radial growth, as mentioned above. The alloy composition in QW is related to equivalent beam ratios during the growth. The spontaneous alloy composition adjustment, however, also occurs during radial QW NW growth. Heiss *et al.* [89] presented a versatile quantum-dot-in-rod system that reproducibly self-assembles in GaAs/AlGaAs QW NW systems. This phenomenon was also reported in GaAs-based NWs with a core-shell structure [78,90]. The occurrence of the spontaneous alloy composition can be understood because of the capillarity induced by the nonplanarity of the underlying substrate, which compensates for a given growth rate anisotropy among different crystal facets [78,91].

For axial QW NW, in 2002, Gudiksen *et al.* [80] used a laser-assisted catalytic method to grow GaAs/GaP superlattices in single NWs by modulating the reactants. Since then, much research was conducted to discuss the growth of quantum dots in NWs by using the VLS methods [84,85,89,92,93]. The most important thing during the growth of axial QW in NW is to maintain the

droplet when switching the sources. In 2014, Tatebayashi *et al.* [82] obtained highly uniformed, multi-stacked InGaAs/GaAs quantum dots embedded in GaAs NWs by accurate design. In the following year, they demonstrated room-temperature lasing from single NWs containing 50 of such stacked quantum dots. This was achieved by tailoring the emission energies of each quantum dot in the NW for enhanced optical gain [88]. In 2018, Ren *et al.* [86] grew the axial QW with a much more complex structure. Each NW contains six GaAsSb-based multiple superlattices, consisting of ten GaAsSb-rich inserts, which served as the gain medium.

OPTICAL PROPERTY OF GaAs-BASED NWs

This section introduces the optical properties of GaAs NWs. As a direct bandgap semiconductor, GaAs materials have extensively widespread optical application potential. There, however, are still some problems with GaAs-based NWs that limit the application in NW lasers such as serious surface nonradiative recombination and lower exciton binding energy. We reviewed several methods that improve the optical properties of GaAs-based NWs such as passivation, doping, and QW structures.

Optical properties of GaAs NWs

GaAs has a direct bandgap of about 1.426 eV (the wavelength is about 870 nm) at room temperature (300 K) [94]. The direct and small bandgap of GaAs makes it important for near-infrared optical applications. The exciton binding energy of GaAs, however, is only about 5 meV [17,94], which is far smaller than the room-temperature thermal energy (25 meV at 300 K), limiting its application at high temperatures.

As mentioned above, bulk GaAs only shows ZB structure. However, when the dimension reduces, a metastable WZ structure exists. The alternate appearance of two crystalline phases in the same NW will form a type-II QW structure due to different band edges, as illustrated in Fig. 1c. In 2009, Spirkoska *et al.* [35] synthesized GaAs ZB/WZ heterostructure NWs with different average crystal phase ratios. They found that the emission peaks located at different positions, as illustrated in Fig. 2a, are attributed to the different quantum confinement effects related to the QW thicknesses. In 2013, Graham *et al.* [95] investigated the temperature-dependent optical properties of excitons in GaAs NWs containing ZB/WZ heterostructures. The S-shaped temperature dependence indicates exciton redistribution among states within the polytypic wires. Due to the lower quantum efficiency of the type-II structure, GaAs NWs with high crystal quality and pure phases are needed to achieve NW lasing.

Optical properties of doped GaAs NWs

Doping is known as an effective method that can modulate the optical and electrical properties of semiconductors. In 2013, Sager *et al.* [57] investigated the recombination dynamics in single GaAs NWs with an axial p-n heterojunction by PL and TRPL. The results showed that the Sn-doping (n-type) has a stronger emission intensity and longer PL lifetime than the Zn-doped (p-type) NWs, as indicated in Fig. 2b. The enhanced optical property in the n-doped region is related to the Fermi-level pining at the doped GaAs surface, causing the band bending at the surface and decreasing the surface-related nonradiative recombination. A similar phenomenon was also reported in shelled Si-doped (n-type) GaAs NWs by Boland *et al.* [61], which exhibited longer photocurrent lifetimes. The photocurrent lifetimes of C-doped (p-type) NWs, however, decrease faster at the beginning because of the diffusion of photogenerated electrons toward the defective surface. Then, because of the limitation of the holes caused by the band bending, the attenuation of the optical conductivity slows down. In 2016, Burgess and co-workers [56] employed Zn dopant to increase the radiative recombination rate. A radical increase in radiative efficiency demonstrates room-temperature lasing in doped GaAs NWs without passivation. Recently, they reported the influence of p-type doping on the optical properties of NWs based on a large-scale optical technique [54]. The results show that the optimal doping level is about 1.2×10^{19} cm^{-3}. Above this value, nonradiative recombination *via* the Auger mechanism begins to dominate.

Optical properties of passivated GaAs NWs

GaAs semiconductor NWs suffer from serious surface defects due to their large surface-to-volume ratio. Bare GaAs NWs usually possess a low radiative efficiency and, therefore, are not considered for optical applications [96,97]. In recent decades, many procedures on GaAs surface passivation have been studied. Among these procedures, chemical passivation and core-shell structure are the two popular effective passivation methods.

The chemical passivation method has been widely used for GaAs thin films [98,99]. Sulfide chemical passivation by using water ammonium sulfide ($(NH_4)_2S$) or sodium sulfide (Na_2S) solutions is one of the most useful methods used in NW-based solar cells [100] and other electronic

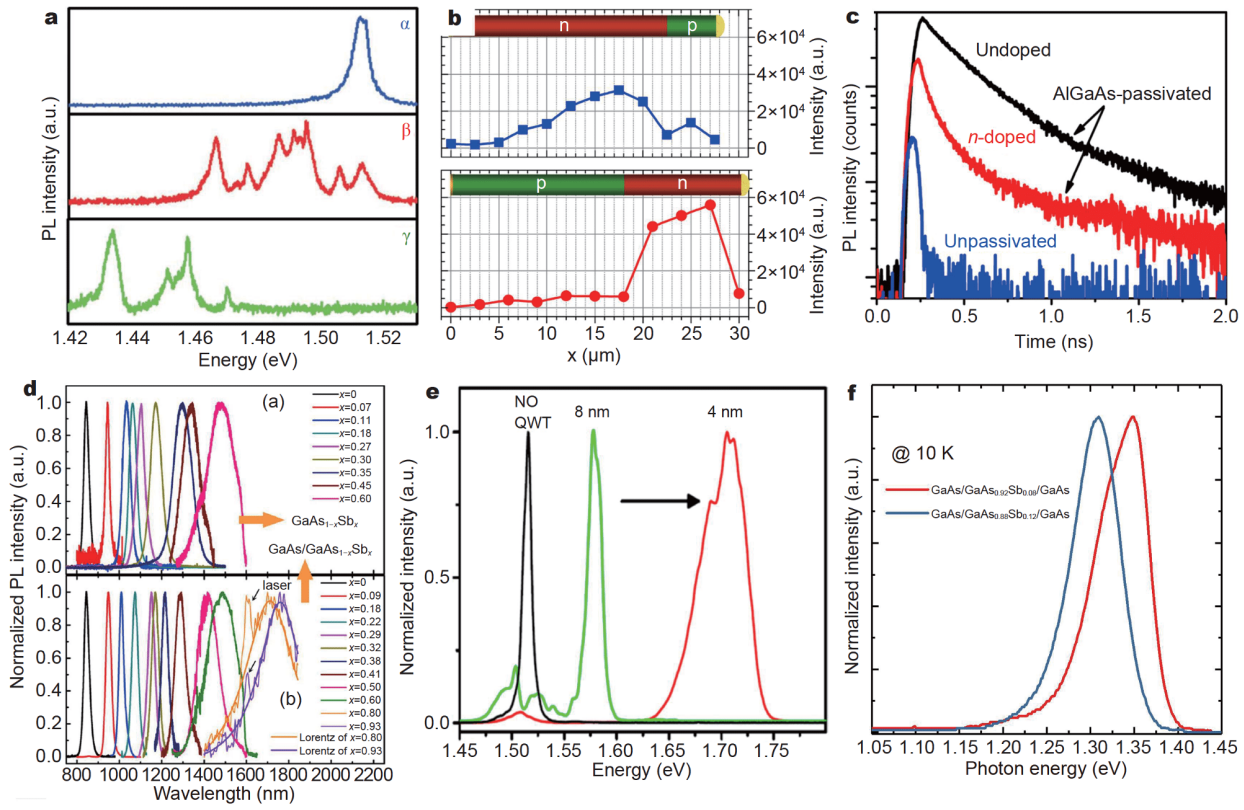

Figure 2 Optical property of GaAs based NWs. (a) PL spectra of WZ/ZB mixed-phase NWs. (The amount of WZ phase gradually increases from top to bottom.) Reproduced with permission from [35]. Copyright 2009, American Physical Society. (b) Comparison of PL intensity of GaAs NWs with different doping types. Reproduced with permission from [57]. Copyright 2013, AIP Publishing. (c) Enhanced GaAs NW PL lifetime by AlGaAs passivation. Reproduced with permission from [113]. Copyright 2012, American Chemical Society. (d) Wavelength tunability through component adjustment in $GaAs_{1-x}Sb_x$ NWs. Reproduced with permission from [119]. Copyright 2017, American Chemical Society. (e) Wavelength tunability due to QW width. Reproduced with permission from [79]. Copyright 2013, American Chemical Society. (f) Wavelength tunability due to alloy composition in QW NW. Reproduced with permission from [76]. Copyright 2019, Royal Society of Chemistry.

devices [101–103]. The principle of sulfide passivation is the removal of native oxide layers and the saturation of dangling bonds by S-ions [104]. The stability of the sulfide passivating layer, however, was not good enough under ambient conditions. In 2015, Alekseev *et al.* [105] reported a nitride surface passivation method. The GaAs NWs treated with the N_2H_2 solution exhibit a 6-fold enhancement of PL intensity. Moreover, the nitride NWs have better stability for the emission intensity to only decrease 10% after six months.

The core-shell structure is another commonly used method for passivating GaAs NWs. Various materials that, in general, have a wider bandgap than GaAs are used as the shell to confine the carriers in the core, such as AlGaAs [8,9,74,79,96,97,106–113], GaInP [114], AlInP [90,115], GaAsP [10], and GaNAs [116]. AlGaAs-GaAs core-shell structured NWs were first reported in 2004 by Tateno *et al.* [109]. The GaAs NWs passivated by AlGaAs show a sharp PL emission (~730 nm) at low temperature, which is ascribed to the excitonic recombination. The exciton peak position confirms that the surface recombination in GaAs NWs was suppressed. In 2010, Demichel *et al.* [97] compared the PL intensity of NWs with or without an AlGaAs capping shell as a function of the diameter. They found that the optical properties of unpassivated NWs are governed by Fermi-level pining, and the passivation of AlGaAs shells could reduce the nonradiative recombination on the surface and that the surface recombination velocity is one order of magnitude lower than unpassivated samples. Previous research showed that the AlGaAs shell could increase the PL lifetime of NWs, as shown in Fig. 2c, which is also related to the reduction of nonradiative recombination on the surface [96,108,113]. In 2005, Sköld *et al.* [114] synthesized GaAs-$Ga_xIn_{1-x}P$ ($0.34 < x < 0.69$) core-shell NWs. The emission efficiency increased by two to three orders

due to shell passivation. Then, they used AlInP as a shell to passivate the GaAs NWs [90]. The emission efficiency of the GaAs core was enhanced at least two orders of magnitude by removing the surface states.

The GaAs/GaAsP core-shell NWs were reported by Hua and co-workers [10]. The PL emission intensity of GaAsP-passivated NWs is stronger than that of bare GaAs NWs over two orders of magnitude. Because of the surface passivation, low-temperature NW laser emission is realized. Lattice mismatch must be considered in shell selection. The lattice constant mismatch of the core and shell materials will induce strain and defect at the interface, influencing the band structure of the core material. AlGaAs is the most commonly used shell material because its lattice constant (~5.656 Å) is almost the same as that of GaAs material (~5.653 Å). In general, another thin GaAs capping layer outside the GaAs-AlGaAs core-shell structure is needed due to the easy oxidation of AlGaAs in the air [106,108]. In addition to various shell materials, the thickness of the shell will also affect the optical properties of the NWs. In 2013, Jiang *et al.* [107] investigated the effect of the AlGaAs shell thickness on the minority carrier lifetime in the GaAs core. They found that when the shell thickness is less than 15 nm, the PL lifetime increases when the AlGaAs shell thickness increases, which is related to the reducing tunneling probability of carriers through the AlGaAs shell. When the thickness of the shell exceeds 15 nm, the PL lifetime is related to the growth quality of the shell.

Wavelength tunability of GaAs-based alloy NWs

Continuous wavelength tunability is one of the critical requirements for advanced optoelectronic devices. The composition adjustment in alloyed NWs is a direct method to achieve this goal. In 2004, Mårtensson *et al.* [117] grew GaAsP ternary NWs, which allowed for wavelength adjustment in variable composition NWs. In 2005, Sköld and co-workers [114] synthesized GaAs-$Ga_xIn_{1-x}P$ ($0.34 < x < 0.69$) core-shell NWs. By adjusting the shell composition, the bandgap of the material was tuned over a range of 240 meV. In 2011, Chen *et al.* [118] grew core-shell NWs with an InGaAs core. By varying the indium composition from 12% to 20%, they achieved wavelength control of on-chip nano-lasers over a ~50 nm range. In 2017, Li *et al.* [119] reported the near full composition range $GaAs_{1-x}Sb_x$ NWs. As shown in Fig. 2d, the emission wavelength of the $GaAs_{1-x}Sb_x$ NWs is tunable from 844 nm (GaAs) to 1760 nm ($GaAs_{0.07}Sb_{0.93}$). $GaAs_{1-x}Sb_x$ with $0 < x < 0.6$ can be grown directly on a Si substrate, while higher composition GaAsSb can be grown through a GaAs/$GaAs_{1-x}Sb_x$ core-shell structure.

QW structure in GaAs-based NWs

Many parameters such as the number, width, and alloy composition of the QW can be adjusted, facilitating the regulation of the optical properties of NWs. QW in NWs provides a new way to achieve the emission tunability and improve the optical gain of GaAs-based NWs. Moreover, the exciton binding energy of GaAs can be increased in QWs because of the quantum confinement effect [120,121]. In 2013, Fickenscher *et al.* [79] studied the optical property of the GaAs/AlGaAs core-multi-shell NWs with different QW thicknesses. The emitted photon energy of the 8 nm QW NW were located at 1.58 eV (~785 nm), which is 60 meV higher than the core GaAs emission, while the peak position of 4 nm QW NW located at 1.7 eV (~730 nm), were nearly 200 meV (~55 nm) higher than the core emission (Fig. 2e). This result confirms that the QW thickness could affect the emission wavelength of QW NWs. We grew GaAs/GaAsSb/GaAs coaxial single QW NWs with different Sb compositions [76]. Fig. 2f shows the PL emission. It is found that with Sb molar fractions increasing from 8 to 12%, the PL emission changes from 1.35 to 1.31 eV (~918 to 947 nm) at 10 K, while the temperature stability improves [76]. The deeper QW is created for higher Sb compositions, which provides more effective confinement for carriers in the quasi-type-II band structure. The composition in the QW also facilitates the adjustment of the NWs lasing wavelength, which will be discussed in the next section.

LASING FROM GaAs-BASED NWs

In recent years, the research of GaAs NWs laser achieved great progress. This section focuses on the realization of GaAs-based NW lasing through passivation, doping, and novel structures. The 1D structure of NWs has natural advantages for lasing because the NW can function as both the optical cavity and gain medium, simultaneously. The reasons limiting the lasing from GaAs-based NWs were mentioned above, namely the worse crystal quality of the NWs and the serious surface nonradiative recombination. After solving these problems, lasing from GaAs NWs can be achieved. NWs have better strain tolerance due to their small size, so complex structures can be designed and manufactured. The development of some other forms of NW lasing will be also discussed.

Cavity mode of NW lasers

Lasers working in UV and visible regions have developed

rapidly, proving the feasibility of NW lasers. Due to the 1D structure, the F-P cavity has been commonly observed in NW lasers [8–10,112,116,122], as shown in Fig. 3a. In 2007, Hua *et al.* [123] reported the F-P microcavity from a single GaAs NW. The cavity was formed along the length of the NW with both ends acting as reflecting mirrors. At a lower temperature, a series of periodic peaks were observed in the PL spectra, ranging from 830 to 940 nm, which was unrelated to excitation power. This result indicates that the high refractive index difference between the GaAs-based material and the surrounding environment can form an F-P cavity where photons can multiply. They attributed the absence of lasing to nonradiative recombination on the surface of the NWs. Later, they grew GaAs/GaAsP NWs to solve the problem of surface states [10]. Thanks to its high crystal quality and effective surface passivation, optically pumped lasing was achieved at low temperatures. In addition to the F-P cavity, laser cavities such as whispering gallery mode were also observed in GaAs-based NWs.

In 2011, Chen *et al.* [118] demonstrated the first room-temperature GaAs-based nano-laser grown on silicon. They found that the lasing shows a special helically propagating mode, as illustrated in Fig. 3b, where both radius and length determine cavity resonances. The strong feedback of helical modes allows for lasers in NWs. Lasing of NWs in this mode, however, requires larger diameter and smoother surface topography. In addition to the cavity formed in single NWs, there is also photonic crystal (PhC) lasers formed by NW arrays. In 2011, Scofield and co-workers [124] grew GaAs/InGaAs/GaAs axial heterostructure nanopillar arrays using the selective area growth method. The thorough accurate growth of gain medium within the cavity, realizes room-temperature lasing under pulsed laser pumping, as shown in Fig. 3c. In the PhC cavities, both the position and diameter of the pillar determine the cavity resonance. To realize such a PhC laser, it is necessary to have an accurate design and much more complicated processes to grow the structure, which increases the process difficulty and production cost of NW lasing. In addition to these three cavities, other forms of laser cavities were reported in other materials such as coupling cavities [125–127] and random cavities [128–130]. Among different types of cavities, the F-P cavity is most commonly used for GaAs-based NW lasers due to the 1D advantage.

Threshold reduction of GaAs-based NW lasing

To achieve GaAs-based NW lasing with a low threshold, the optical gain of GaAs material must be increased. The core-shell structure is commonly used to solve this problem. The first GaAs-based NW lasing was reported in 2009 by Hua *et al.* [10]. By covering the GaAs NW core with a GaAsP shell, optically pumped lasing was achieved at low temperatures. They also studied power-dependent and temperature-dependent emissions of NW lasing. A blue shift of lasing peak was observed as pump power increased, which is related to the band bending in the heterostructure. As for the temperature-dependent PL spectra, the red shift of the lasing wavelength is weaker than that of the GaAs bandgap energy, which is attributed to the temperature-dependent variation of the refractive index.

In 2013, Saxena and co-workers [8] reported the optical pumped room-temperature GaAs NW lasers. In this work, the AlGaAs shell was used to reduce the surface nonradiative recombination. To prevent the oxidation of AlGaAs, a GaAs cap layer was grown on the outer layer.

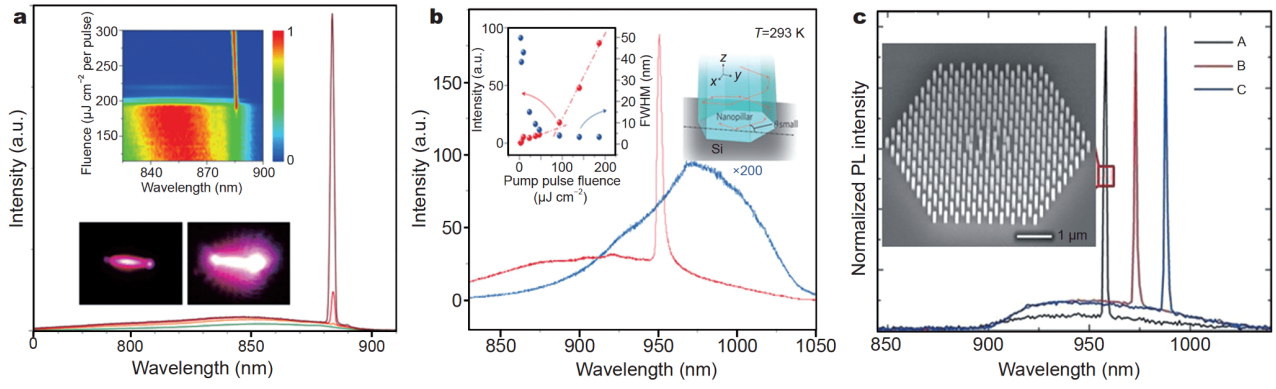

Figure 3 Various cavity geometries of GaAs-based NW lasers. (a) F-P cavity mode. Reproduced with permission from [8]. Copyright 2013, Springer Nature. (b) Helically propagating cavity modes. Reproduced with permission from [118]. Copyright 2011, Springer Nature. (c) Photonic crystal cavity. Reproduced with permission from [124]. Copyright 2011, American Chemical Society.

The authors also investigated the structural design of the GaAs NW laser. For NW lasing, the number of guided modes supported is depended on the NW diameters and the index of the substrate. To effectively confine light inside the NW, it must be placed on a substrate with a smaller reflective index, such as SiO_2 (n = 1.45). In this configuration, the NW behaves as an F-P cavity, as illustrated in Fig. 4a. The large dielectric contract between the NW and the surrounding allows the NW to guide the photonic modes. By calculating the mode confinement, as shown in Fig. 4b, they found that the diameter of the NWs must be bigger than 160 nm to confine the lowest-order guided mode. The effective index for guided modes is closely related to the NW diameter, that is, a larger NW diameter brings a bigger effective index and better-guided mode confinement. Fig. 4c and d show the threshold gain of the supported modes in NW *versus* diameter to achieve a lower threshold. The diameter of the NW must be bigger than 330 nm. A necessary condition for NW lasers is that the round-trip gain for the guided mode inside the NW should be larger than the round-trip losses. Since the optical loss comes from the mirror losses at the end facets of the NW, the gain medium must be long enough to get sufficient amplification [72]. This implies that to achieve NW lasing, longer NWs are needed. Under the condition of ensuring the quality of growth, the length of the NW is inversely proportional to the threshold. Their research provides a reference for the design of NW lasers.

In the same year, Mayer *et al.* [9] also achieved room-temperature lasing of GaAs NWs (Fig. 5a). They also used GaAs/AlGaAs/GaAs core/shell/cap structure. The diameter of the GaAs core is 340 nm, while the thickness of AlGaAs shell is 5 nm, and capped by a 5-nm thick GaAs layer. The length of the NWs is longer than 10 μm. Fig. 5b shows the image of the NW emission above the threshold. The interference fringes around the NW end-face can be observed, while the spontaneous emission from the NW body is weak. This indicates that the lasing comes from the F-P cavity formed by the 1D NW. Furthermore, they studied the temperature-dependent properties of NW lasers and observed multimode lasing at temperatures above 220 K (Fig. 5c), indicating that the reduced peak gain and broadening of the gain spectrum are comparable to the mode spacing at elevated temperatures.

In 2014, Sun *et al.* [131] demonstrated room-temperature lasers in InGaAs/InGaP core-shell nanopillars. They compared the optical properties of unpassivated, GaAs-passivated, and InGaP-passivated InGaAs nano-

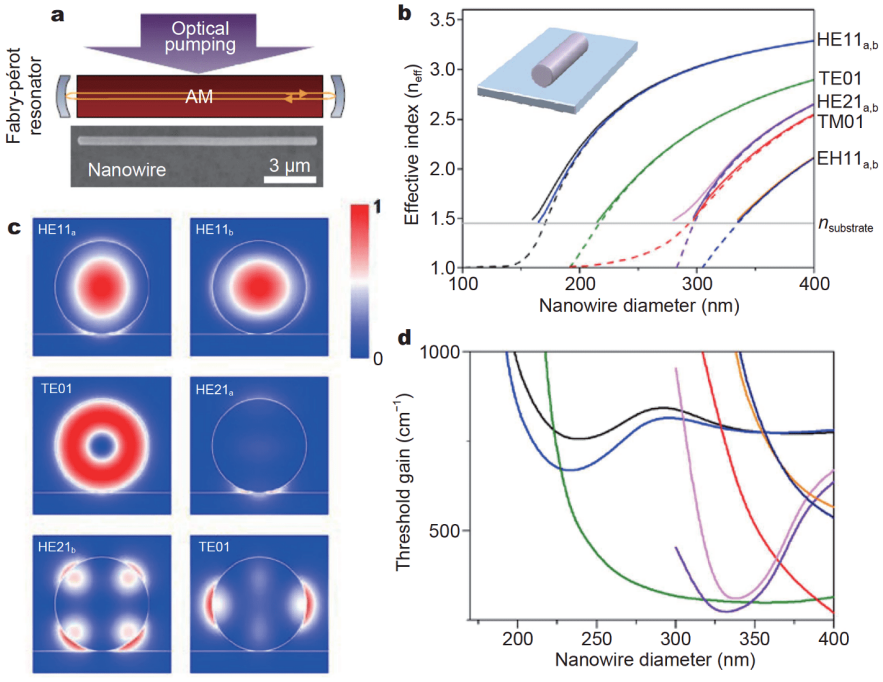

Figure 4 Design of single GaAs NW Laser. (a) The schematic diagram of F-P cavity in NW. Reproduced with permission from [14]. Copyright 2018, IOP Publishing. (b) Relationship between effective refractive index and diameter of different guided modes in NWs. (c) Electric field intensity profiles of different guided modes in NW. (d) Threshold gain of supported modes *versus* NW diameter. Reproduced with permission from [8] Copyright 2013, Springer Nature.

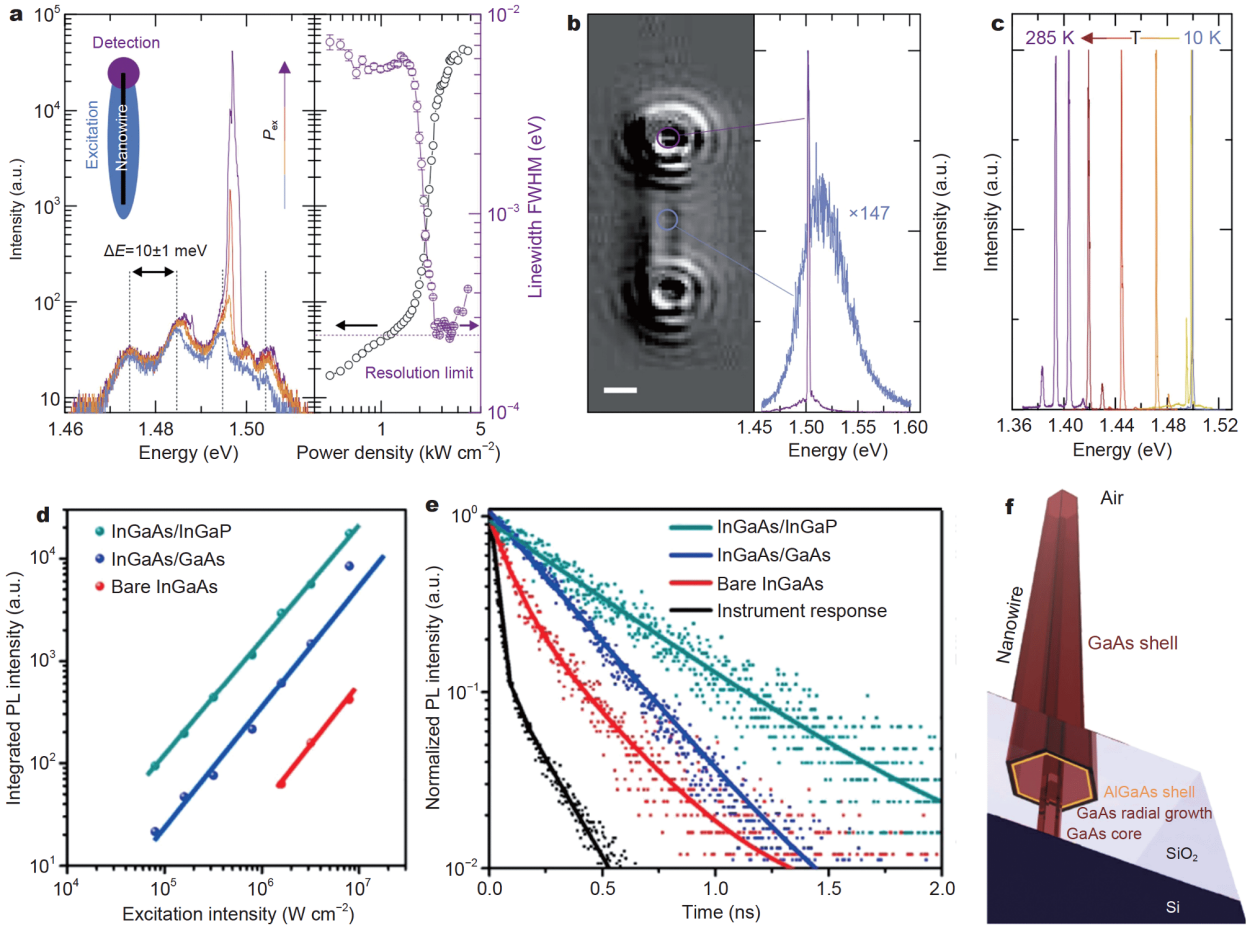

Figure 5 Lasing from individual GaAs-AlGaAs core-shell NWs. (a) Power-dependent spectra above and below the threshold. (b) Emission spectra from the top and side walls of the NWs, indicates F-P cavity mode lasing. (c) Temperature-dependent emission spectra. With temperature increase, the laser change from single-mode to multi-mode. Reproduced with permission from [9]. Copyright 2013, Springer Nature. (d) The PL intensity is enhanced by ~10 and ~50 times, respectively. (e) Corresponding TRPL decay for InGaAs nanopillars with GaAs and InGaP passivation layers. Reproduced with permission from [131]. Copyright 2014, American Chemical Society. (f) Schematic representation of the GaAs-AlGaAs core-shell NWs grown on silicon with an interlayer. Reproduced with permission from [122]. Copyright 2016, American Chemical Society.

pillars. The results show that the PL intensity is enhanced by ~10 times for GaAs-passivated and ~50 times for InGaP-passivated compared with the bare InGaAs nanopillars (Fig. 5d). Moreover, the effective lifetime of InGaAs/InGaP pillars is enhanced by a factor of five compared with the unpassivated ones (Fig. 5e). Different improvements were attributed to the larger band offset between InGaP and InGaAs than that of the GaAs and InGaAs structures. In the same year, Wei and co-workers [112] grew GaAs/AlGaAs core-shell NWs and observed lasing emission at room temperature. By careful design of the length and cavity of the NW, the lasing wavelength can change from 853.56 to 882.48 nm. Among those results, F-P mode lasing from NWs on silicon is challenging to achieve due to the poor modal reflectivity at the NW-silicon interface.

In 2016, a new structure was proposed and realized to solve this problem. Mayer *et al.* [122], as illustrated in Fig. 5f, grew a SiO_2 interlayer between the NW and the silicon substrate. The GaAs/AlGaAs core-shell NW with free-standing, vertical geometry on silicon has high spontaneous emission coupling (β) factors. Since SiO_2 has a smaller refractive index, the guided mode can be confined in the NW, which brings the low threshold pump power of only 11 ± 1 pJ per pulse and a remarkably high spontaneous emission coupling factor of β = 21%. Moreover, since the NW laser is in direct contact with the substrate, a doped low-refractive-index dielectric layer can be designed to form a heterojunction with the doped NWs. This structure provides a new idea for electrically

driven NW lasers working on silicon. They also demonstrated the single-mode continuous-wave lasing from individual GaAs-AlGaAs core-shell NWs working at low temperatures [110]. The thermal effect is the biggest problem toward realizing the NW laser working under continuous optical pumping. To solve this problem, previously reported GaAs-based NW lasers are realized by pulsed laser pumping, which can reduce the thermal effect induced during excitation. The quality of NW growth must be improved and effective passivation methods must be used to reduce nonradiative recombination. In 2017, Chen *et al.* [116] demonstrated GaAs/GaNAs core-shell NW lasing. Their results showed that GaNAs is also an excellent material for passivating GaAs NWs to reduce surface nonradiative recombination. The most mature passivation method developed so far is using GaAs/AlGaAs/GaAs core-shell-cap NWs. This is due to the almost negligible lattice mismatch between AlGaAs and GaAs, which shows convenience during high-quality NW growth.

Another way to reduce the nonradiative recombination is to increase the efficiency of radiative recombination. In 2016, Burgess and co-workers [56] employed impurity doping to enhance the radiative efficiency and achieved lasing in unpassivated NWs. As shown in Fig. 6a, Zn-doping leads to a ZB twining superlattice structure. The external quantum efficiency of the doped NW is two orders of magnitude higher than that of the undoped NW. Due to the increasing differential gain and reducing the transparency carrier density, lasing was achieved at room temperature, as shown in Fig. 6b. The enhanced optical property indicates a significant increase in radiation efficiency but the room-temperature lifetime of the doped samples is still in the same order of picoseconds (Fig. 6c). Doping, therefore, cannot effectively reduce the nonradiative recombination that occurs on the surface of NWs. The increase in PL intensity, therefore, is related to the increase in radiation recombination efficiency. With

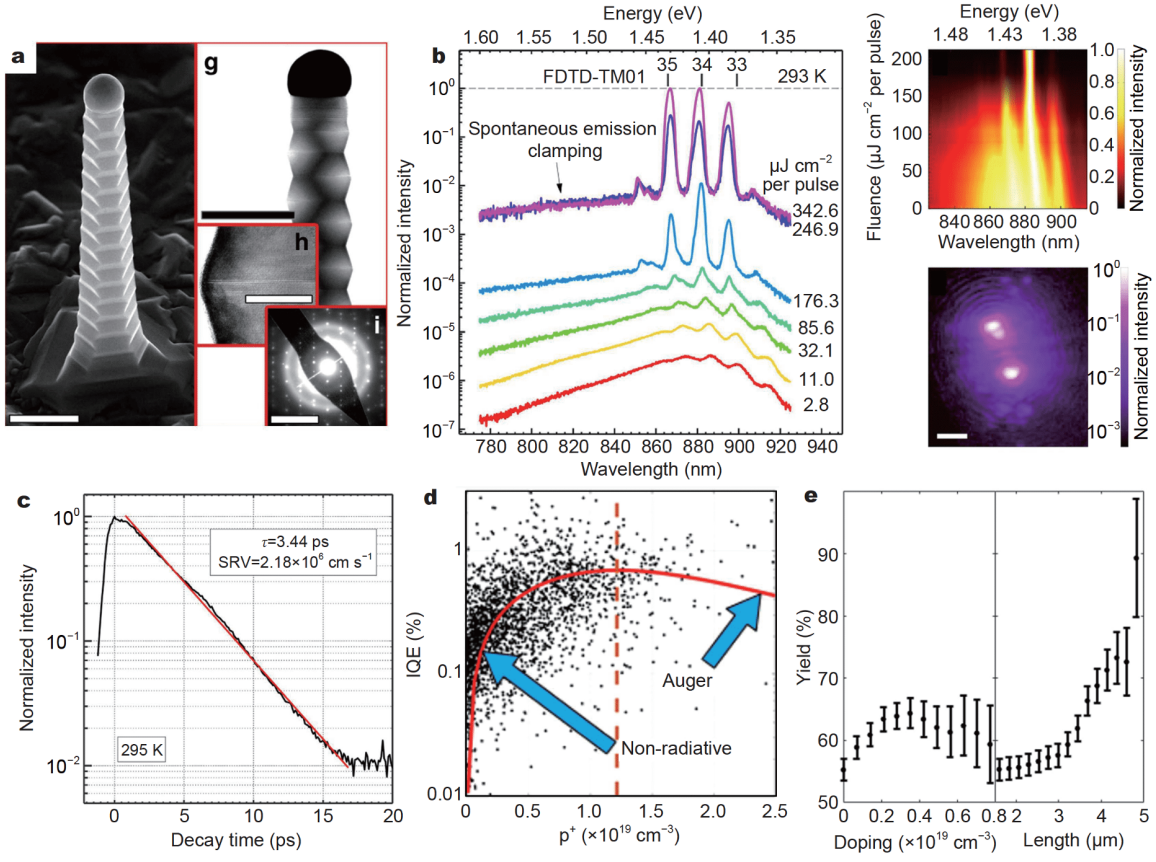

Figure 6 Lasing from doped GaAs NWs. (a) Morphology of doped GaAs NWs. (b) Power-dependent spectra above and below the threshold and logarithmic map of a composite optical image above threshold. (c) Carrier lifetime of doped GaAs NWs. Reproduced with permission from [56]. Copyright 2016, Springer Nature. (d) Internal quantum efficiency as a function of doping concentration. (e) Lasing yield as a function of doping concentration and NW length. Reproduced with permission from [54]. Copyright 2019, American Chemical Society.

the picosecond carrier lifetime, doped NW lasers are more suitable for applications in high-speed devices. In 2019, Alanis *et al.* [54] investigated the effects of doping levels and NW length on NW lasing thresholds. Fig. 6d and e show the statistical results of the optical properties of 975 NWs with different doping concentrations and lengths. For higher doping levels, the PL intensity is enhanced, and the improvement in functional performance is further confirmed by the lower laser threshold and the high laser yield of the NWs with a higher doping level. Excessive doping, however, will induce Auger recombination and degrade the optical performance of NWs. In the F-P cavity, longer NWs bring bigger optical gain, which will lower the lasing threshold and increase the lasing yield.

Optical gain improvement and lasing tunability

The QW structure in NWs provides more adjustability for NW lasing. The optical gain of a QW is related to the number of wells, and the lasing wavelength can be adjusted by the width of the well and the composition of the alloy in the well.

In 2016, Stettner *et al.* [65] compared the lasing behavior of a single QW (SQW) and multiple QW (MQW) in coaxial NWs. In SQW, a single GaAs layer (~8 nm) is sandwiched between AlGaAs barriers, while the MQW consists of seven-period GaAs QWs (8 nm) separated by AlGaAs layers (10 nm). Their laser performances show different trends. In the MQW NW, the lasing shifted to higher photon energy with increasing excitation power. The blue shift is attributed to band filling effects. The threshold measured in MQW NWs is about 6.5 times smaller than that in SQW. Overall, in weakly coupled QW separated by high barriers, each well is almost independent. The density state of electrons increases with the number of wells, resulting in bigger optical gain and lower lasing threshold. In the same year, Saxena and co-workers [73] presented the design of the F-P type NW cavities with radial GaAs/AlGaAs MQW active regions. They proved that to obtain the lowest threshold in a given NW structure, suitable QW numbers and QW widths are needed. The laser mode is determined by the placement of the QW rather than the diameter of the NW. By modeling the loss in the GaAs/AlGaAs QW structure, it is found that for all diameters larger than 240 nm, the TE_{01} mode has the smallest modal loss, as shown in Fig. 7a, which is different from the NW with the core as the active region [8]. The absorbing passive region in MQW causes this difference. The TE_{01} mode has the lowest loss and is related to its poor overlap of intensity profile with the passive region. In their design, the diameter of the NW must be bigger than 400 nm to minimize the TE_{01} mode loss. To increase the modal gain, multiple QWs can be used but the barriers must be thick enough to avoid coupling. Fig. 7b shows the model loss of the TE_{01} mode with different well numbers and well thicknesses. It is found that in NWs with a diameter of 420 nm, the optimal number of wells is eight and the optimal well thickness is 4 nm. Although the gain is proportional to the number of wells, when having more than eight pairs of QWs, the thickness of the barrier layer is not enough to separate each QWs. They grew MQW NWs as designed and got NW lasing with a low threshold. The experimental results agree well with the simulation (Fig. 7c and d). In 2017, Yuan *et al.* [68] studied the growth and optical property of GaAsSb/AlGaAs SQW. Because of the higher growth quality and support for the F-P cavity mode, they observed strongly stimulated radiation. Polarization-dependent PL and simulation results confirm that the periodic peaks are the TE_{01} mode.

The wavelength tunability of GaAs-based NW lasing was first reported in 2011. Chen *et al.* [118] changed the In composition of InGaAs/GaAs core-shell NWs between ~12% and 20% and realized a 50 nm tunability of lasing wavelength. The introduction of the QW structure in NWs provides more advantages for NW laser wavelength tunability. In the QW structure, modifying the width of the QW can realize a small range of lasing wavelengths. Altering the alloy composition of the active region can achieve wider laser wavelength tunability. In 2017, Lu *et al.* [71] grew InGaAs/InP NWs. When the thickness of the QW reduces from 5 to 1.3 nm, the lasing wavelength blue shifts approximately 200 nm. With the increase of In composition, the lasing wavelength can shift from ~1200 to 1300 nm. Similar observations were also reported in InGaAs/InP MQW NWs. In 2018, Stettner *et al.* [67] observed lasing in GaAs/(In, Al)GaAs MQW NWs. When the In composition is adjusted between 0% and 40% for InGaAs, the lasing peak position can be changed from 1.55 to 1.36 eV (~800 to 912 nm). By controlling the growth temperature of the shell, the doping of In will increase and the alloy intermixing in the MQW can be reduced. Then, the lasing peak energy can be further adjusted to 1.18 eV (~1050 nm), as shown in Fig. 8a. The modulation of the lasing wavelength caused by the composition change was also reported in the axial QW structure. In 2018, Ren and co-workers [86] demonstrated a single-mode NW laser with six GaAsSb-based multiple superlattices, where each superlattice consists of ten GaAsSb-rich inserts, as indicated in Fig. 8b. By

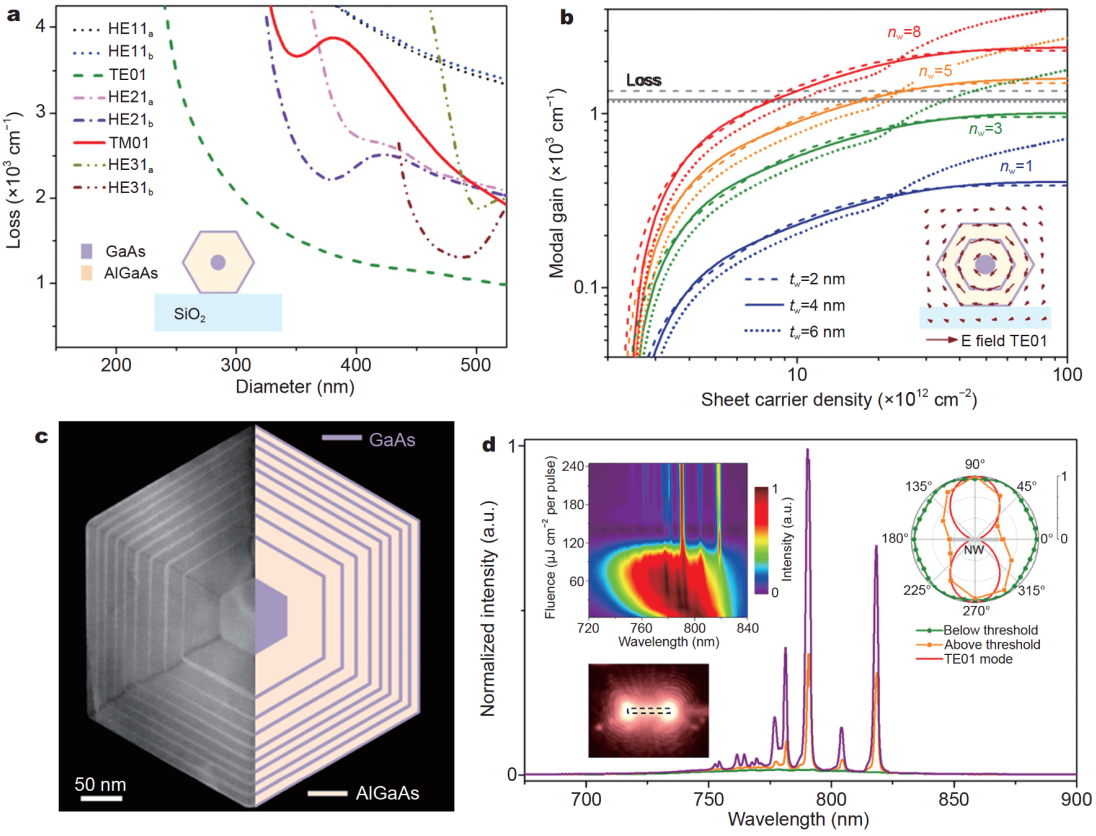

Figure 7 Design for GaAs multi-QW NW laser. (a) Modal loss as a function of QW NW diameter. (b) Modal gain of QWs NWs with different QW numbers and widths. (c) Structural characterization of GaAs multi-QW NWs. (d) Room-temperature lasing characteristics. Reproduced with permission from [73]. Copyright 2016, American Chemical Society.

changing the Sb composition between 1% and 8%, the laser emission wavelength is adjusted between 880 and 980 nm.

Plasmonic GaAs-based NW lasing

A promising way to further miniaturize NW lasers is to combine the material with surface plasmons. In 2016, Ho *et al.* [87] introduced the first quantum dot-based plasmonic laser. The GaAs/AlGaAs core-shell NW containing InGaAs quantum dots was placed directly on silver film. Although the diameter of the NW is smaller than the minimum size of the restricted gain mode, they observed the laser emission due to the coupling between the quantum dots and the surface plasmon. In 2017, Bermúdez-Ureña and co-workers [132] reported the realization of hybrid photonic devices consisting of NW lasers integrated with V-groove plasmonic waveguides. Theoretical considerations suggest that the observed lasing is enabled by a waveguided hybrid photonic-plasmonic mode. In addition to surface plasmon lasers, in 2018, Ha *et al.* [133] demonstrated directional lasing in active dielectric nano-antenna arrays by coupling leaky resonances excited in GaAs nanopillars.

SUMMARY AND PROSPECTS

In conclusion, there have been significant achievements in the growth of GaAs-based NWs with high crystal quality and complex structures, which is essential for achieving infrared NW lasers. Controlling crystallographic phase purity is a major challenge for GaAs NW growth based on the VLS mechanism. Currently, TPL theory is used to explain the appearance of the metastable WZ phase. The growth of pure-phase GaAs NWs can be realized by controlling the temperature and V:III equivalent beam ratio during the growth process. There have also been great advances in the regulation of NW properties such as doping and QW structures. The optical property of GaAs-based NWs was improved significantly. GaAs-based NWs suffer from serious surface states due to the large surface-to-volume ratio. This can be solved by

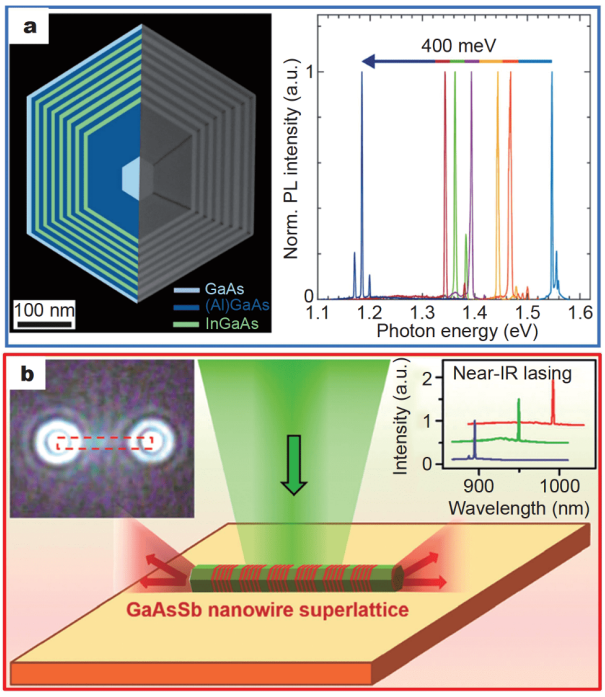

Figure 8 Wavelength tunability by QWs in NWs. (a) Laser wavelength tunability in InGaAs/AlGaAs multilayer coaxial QW structure. Reproduced with permission from [67]. Copyright 2018, American Chemical Society. (b) Laser wavelength tunability in GaAsSb/GaAs dot in rod axial quantum well structure. Reproduced with permission from [86]. Copyright 2018, American Chemical Society.

reducing nonradiative recombination by passivation or increasing the radiative recombination by doping. Much research focuses on the continuous wavelength tunability of NW optical properties. Composition adjustments in alloyed NWs and QW structures were used to facilitate the regulation of the optical properties of GaAs-based NWs. By the proper design of the optical cavity and improvement of the optical gain, lasing can be achieved in individual NWs. Complex QW structures in NWs can effectively lower the threshold and allow for the continuous tunability of lasing wavelengths.

Although great progress has been made in GaAs-based NW lasers, there are still some encumbrances that must be overcome to fully achieve the potential of these lasers. Due to the bad thermal dissipation, most optically pumped NW lasers are realized by pulse pumping, which could produce sufficient instantaneous carrier density with lower thermal effects. Continuous nanowire lasers, however, are required in optical integrated devices. To reduce the heat generated in NWs and achieve continuous-wave lasing at room temperature, effective and low refractive index heat sinking are required. In 2018, Valente *et al.* [134] demonstrated a technique to transfer large-area NW arrays to flexible substrates. They observed that the PL emission was improved due to the modification of the surface states. The transfer technology allows the achievement of GaAs-based nanowire lasing on flexible substrates. Most importantly, electrically pumped GaAs-based NW lasers are still the biggest challenge. Electrical injection is a critical part of any semiconductor laser, especially for nanophotonic integrated systems or on-chip systems. To achieve electrical injection, one of the key issues is the design of a favorable injection configuration. QW can potentially form a p-n junction that allows for the higher concentration of electrons and holes to be injected, which provides conditions for electrically pumped GaAs-based nanowire lasing.

Received 31 January 2020; accepted 5 March 2020; published online 15 April 2020

1 Koblmüller G, Mayer B, Stettner T, *et al.* GaAs–AlGaAs core–shell nanowire lasers on silicon: invited review. Semicond Sci Technol, 2017, 32: 053001
2 Thomson D, Zilkie A, Bowers JE, *et al.* Roadmap on silicon photonics. J Opt, 2016, 18: 073003
3 Maiman TH. Stimulated optical radiation in ruby. Nature, 1960, 187: 493–494
4 Huang MH, Mao S, Feick H, *et al.* Room-temperature ultraviolet nanowire nanolasers. Science, 2001, 292: 1897–1899
5 Johnson JC, Choi HJ, Knutsen KP, *et al.* Single gallium nitride nanowire lasers. Nat Mater, 2002, 1: 106–110
6 Agarwal R, Barrelet CJ, Lieber CM. Lasing in single cadmium sulfide nanowire optical cavities. Nano Lett, 2005, 5: 917–920
7 Xing G, Luo J, Li H, *et al.* Ultrafast exciton dynamics and two-photon pumped lasing from ZnSe nanowires. Adv Opt Mater, 2013, 1: 319–326
8 Saxena D, Mokkapati S, Parkinson P, *et al.* Optically pumped room-temperature GaAs nanowire lasers. Nat Photon, 2013, 7: 963–968
9 Mayer B, Rudolph D, Schnell J, *et al.* Lasing from individual GaAs-AlGaAs core-shell nanowires up to room temperature. Nat Commun, 2013, 4: 2931
10 Hua B, Motohisa J, Kobayashi Y, *et al.* Single GaAs/GaAsP coaxial core−shell nanowire lasers. Nano Lett, 2009, 9: 112–116
11 Chin AH, Vaddiraju S, Maslov AV, *et al.* Near-infrared semiconductor subwavelength-wire lasers. Appl Phys Lett, 2006, 88: 163115
12 Gao Q, Saxena D, Wang F, *et al.* Selective-area epitaxy of pure wurtzite InP nanowires: high quantum efficiency and room-temperature lasing. Nano Lett, 2014, 14: 5206–5211
13 Maslov AV, Ning CZ. Reflection of guided modes in a semiconductor nanowire laser. Appl Phys Lett, 2003, 83: 1237–1239
14 Röder R, Ronning C. Review on the dynamics of semiconductor nanowire lasers. Semicond Sci Technol, 2018, 33: 033001
15 Eaton SW, Fu A, Wong AB, *et al.* Semiconductor nanowire lasers. Nat Rev Mater, 2016, 1: 16028
16 Hill MT, Gather MC. Advances in small lasers. Nat Photon, 2014, 8: 908–918

17 Zhang Y, Saxena D, Aagesen M, *et al.* Toward electrically driven semiconductor nanowire lasers. Nanotechnology, 2019, 30: 192002
18 Couteau C, Larrue A, Wilhelm C, et al. Nanowire lasers. Nanophotonics, 2015, 4: 90–107
19 Yang P, Yan R, Fardy M. Semiconductor nanowire: What's next? Nano Lett, 2010, 10: 1529–1536
20 Quan LN, Kang J, Ning CZ, *et al.* Nanowires for photonics. Chem Rev, 2019, 119: 9153–9169
21 Ning CZ. Semiconductor nanowire lasers. Semiconduct Semimet. 2012, 86: 455–486
22 Dasgupta NP, Sun J, Liu C, *et al.* 25th anniversary article: Semiconductor nanowires—Synthesis, characterization, and applications. Adv Mater, 2014, 26: 2137–2184
23 Güniat L, Caroff P, Fontcuberta i Morral A. Vapor phase growth of semiconductor nanowires: key developments and open questions. Chem Rev, 2019, 119: 8958–8971
24 Fortuna SA, Li X. Metal-catalyzed semiconductor nanowires: a review on the control of growth directions. Semicond Sci Technol, 2010, 25: 024005
25 Lu W, Lieber CM. Semiconductor nanowires. J Phys D-Appl Phys, 2006, 39: R387–R406
26 Fan HJ, Werner P, Zacharias M. Semiconductor nanowires: From self-organization to patterned growth. Small, 2006, 2: 700–717
27 Barrigón E, Heurlin M, Bi Z, *et al.* Synthesis and applications of III–V nanowires. Chem Rev, 2019, 119: 9170–9220
28 Li A, Zou J, Han X. Growth of III-V semiconductor nanowires and their heterostructures. Sci China Mater, 2016, 59: 51–91
29 Morral AF. Gold-free GaAs nanowire synthesis and optical properties. IEEE J Sel Top Quantum Electron, 2011, 17: 819–828
30 Wagner RS, Ellis WC. Vapor-liquid-solid mechanism of single crystal growth. Appl Phys Lett, 1964, 4: 89–90
31 Rudolph D, Hertenberger S, Bolte S, *et al.* Direct observation of a noncatalytic growth regime for GaAs nanowires. Nano Lett, 2011, 11: 3848–3854
32 Fontcuberta i Morral A, Colombo C, Abstreiter G, *et al.* Nucleation mechanism of gallium-assisted molecular beam epitaxy growth of gallium arsenide nanowires. Appl Phys Lett, 2008, 92: 063112
33 Duan X, Wang J, Lieber CM. Synthesis and optical properties of gallium arsenide nanowires. Appl Phys Lett, 2000, 76: 1116–1118
34 Breuer S, Pfuller C, Flissikowski T, *et al.* Suitability of Au- and self-assisted GaAs nanowires for optoelectronic applications. Nano Lett, 2011, 11: 1276–1279
35 Spirkoska D, Arbiol J, Gustafsson A, *et al.* Structural and optical properties of high quality zinc-blende/wurtzite GaAs nanowire heterostructures. Phys Rev B, 2009, 80: 245325
36 Glas F, Harmand JC, Patriarche G. Why does wurtzite form in nanowires of III-V zinc blende semiconductors? Phys Rev Lett, 2007, 99: 146101
37 Dubrovskii VG, Sibirev NV, Harmand JC, *et al.* Growth kinetics and crystal structure of semiconductor nanowires. Phys Rev B, 2008, 78: 235301
38 Dubrovskii VG. Influence of the group V element on the chemical potential and crystal structure of Au-catalyzed III-V nanowires. Appl Phys Lett, 2014, 104: 053110
39 Dubrovskii VG. Mono- and polynucleation, atomistic growth, and crystal phase of III-V nanowires under varying group V flow. J Chem Phys, 2015, 142: 204702
40 Matteini F, Tütüncüoglu G, Mikulik D, *et al.* Impact of the Ga droplet wetting, morphology, and pinholes on the orientation of GaAs nanowires. Cryst Growth Des, 2016, 5781–5786
41 Tersoff J. Stable self-catalyzed growth of III–V nanowires. Nano Lett, 2015, 15: 6609–6613
42 Dubrovskii VG. Refinement of nucleation theory for vapor–liquid–solid nanowires. Cryst Growth Des, 2017, 17: 2589–2593
43 Mårtensson EK, Lehmann S, Dick KA, *et al.* Simulation of GaAs nanowire growth and crystal structure. Nano Lett, 2019, 19: 1197–1203
44 Lehmann S, Wallentin J, Jacobsson D, *et al.* A general approach for sharp crystal phase switching in InAs, GaAs, InP, and GaP nanowires using only group V flow. Nano Lett, 2013, 13: 4099–4105
45 Joyce HJ, Wong-Leung J, Gao Q, *et al.* Phase perfection in zinc blende and wurtzite III–V nanowires using basic growth parameters. Nano Lett, 2010, 10: 908–915
46 Krogstrup P, Popovitz-Biro R, Johnson E, *et al.* Structural phase control in self-catalyzed growth of GaAs nanowires on silicon (111). Nano Lett, 2010, 10: 4475–4482
47 Kim W, Dubrovskii VG, Vukajlovic-Plestina J, *et al.* Bistability of contact angle and its role in achieving quantum-thin self-assisted GaAs nanowires. Nano Lett, 2018, 18: 49–57
48 Maliakkal CB, Jacobsson D, Tornberg M, *et al. In situ* analysis of catalyst composition during gold catalyzed GaAs nanowire growth. Nat Commun, 2019, 10: 4577
49 Schroth P, Al Humaidi M, Feigl L, *et al.* Impact of the shadowing effect on the crystal structure of patterned self-catalyzed GaAs nanowires. Nano Lett, 2019, 19: 4263–4271
50 de la Mata M, Magén C, Caroff P, *et al.* Atomic scale strain relaxation in axial semiconductor III–V nanowire heterostructures. Nano Lett, 2014, 14: 6614–6620
51 Zhou C, Zheng K, Chen PP, *et al.* Crystal-phase control of GaAs–GaAsSb core–shell/axial nanowire heterostructures by a two-step growth method. J Mater Chem C, 2018, 6: 6726–6732
52 Joyce HJ, Gao Q, Tan HH, *et al.* Twin-free uniform epitaxial GaAs nanowires grown by a two-temperature process. Nano Lett, 2007, 7: 921–926
53 Haraguchi K, Katsuyama T, Hiruma K, *et al.* GaAs p-n junction formed in quantum wire crystals. Appl Phys Lett, 1992, 60: 745–747
54 Alanis JA, Lysevych M, Burgess T, *et al.* Optical study of p-doping in GaAs nanowires for low-threshold and high-yield lasing. Nano Lett, 2019, 19: 362–368
55 Isik Goktas N, Fiordaliso EM, LaPierre RR. Doping assessment in GaAs nanowires. Nanotechnology, 2018, 29: 234001
56 Burgess T, Saxena D, Mokkapati S, *et al.* Doping-enhanced radiative efficiency enables lasing in unpassivated GaAs nanowires. Nat Commun, 2016, 7: 11927
57 Sager D, Gutsche C, Prost W, *et al.* Recombination dynamics in single GaAs-nanowires with an axial heterojunction: n- *versus* p-doped areas. J Appl Phys, 2013, 113: 174303
58 Zhang Y, Sun Z, Sanchez AM, *et al.* Doping of self-catalyzed nanowires under the influence of droplets. Nano Lett, 2018, 18: 81–87
59 Dastjerdi MHT, Fiordaliso EM, Leshchenko ED, *et al.* Three-fold symmetric doping mechanism in GaAs nanowires. Nano Lett, 2017, 17: 5875–5882
60 Czaban JA, Thompson DA, LaPierre RR. GaAs core–shell nanowires for photovoltaic applications. Nano Lett, 2009, 9: 148–154
61 Boland JL, Casadei A, Tütüncüoglu G, *et al.* Increased photo-

conductivity lifetime in GaAs nanowires by controlled n-type and p-type doping. ACS Nano, 2016, 10: 4219–4227
62 Boland JL, Conesa-Boj S, Parkinson P, *et al.* Modulation doping of GaAs/AlGaAs core–shell nanowires with effective defect passivation and high electron mobility. Nano Lett, 2015, 15: 1336–1342
63 Chen X, Wang D, Wang T, *et al.* Enhanced photoresponsivity of a GaAs nanowire metal-semiconductor-metal photodetector by adjusting the fermi level. ACS Appl Mater Interfaces, 2019, 11: 33188–33193
64 Ali H, Zhang Y, Tang J, *et al.* High-responsivity photodetection by a self-catalyzed phase-pure p-GaAs nanowire. Small, 2018, 14: 1704429
65 Stettner T, Zimmermann P, Loitsch B, *et al.* Coaxial GaAs-AlGaAs core-multishell nanowire lasers with epitaxial gain control. Appl Phys Lett, 2016, 108: 011108
66 Zhang Y, Davis G, Fonseka HA, *et al.* Highly strained III–V–V coaxial nanowire quantum wells with strong carrier confinement. ACS Nano, 2019, 13: 5931–5938
67 Stettner T, Thurn A, Döblinger M, *et al.* Tuning lasing emission toward long wavelengths in GaAs-(In,Al)GaAs core–multishell nanowires. Nano Lett, 2018, 18: 6292–6300
68 Yuan X, Saxena D, Caroff P, *et al.* Strong amplified spontaneous emission from high quality $GaAs_{1-x}Sb_x$ single quantum well nanowires. J Phys Chem C, 2017, 121: 8636–8644
69 Yan X, Wei W, Tang F, *et al.* Low-threshold room-temperature AlGaAs/GaAs nanowire/single-quantum-well heterostructure laser. Appl Phys Lett, 2017, 110: 061104
70 Schuster F, Kapraun J, Malheiros-Silveira GN, *et al.* Site-controlled growth of monolithic InGaAs/InP quantum well nanopillar lasers on silicon. Nano Lett, 2017, 17: 2697–2702
71 Lu F, Bhattacharya I, Sun H, *et al.* Nanopillar quantum well lasers directly grown on silicon and emitting at silicon-transparent wavelengths. Optica, 2017, 4: 717–723
72 Alanis JA, Saxena D, Mokkapati S, *et al.* Large-scale statistics for threshold optimization of optically pumped nanowire lasers. Nano Lett, 2017, 17: 4860–4865
73 Saxena D, Jiang N, Yuan X, *et al.* Design and room-temperature operation of GaAs/AlGaAs multiple quantum well nanowire lasers. Nano Lett, 2016, 16: 5080–5086
74 Zhou C, Zhang XT, Zheng K, *et al.* Epitaxial GaAs/AlGaAs core–multishell nanowires with enhanced photoluminescence lifetime. Nanoscale, 2019, 11: 6859–6865
75 Zhang J, Tang J, Kang Y, *et al.* Structural and spectroscopy characterization of coaxial GaAs/GaAsSb/GaAs single quantum well nanowires fabricated by molecular beam epitaxy. CrystEngComm, 2019, 21: 4150–4157
76 Li H, Tang J, Pang G, *et al.* Optical characteristics of GaAs/GaAsSb/GaAs coaxial single quantum-well nanowires with different Sb components. RSC Adv, 2019, 9: 38114–38118
77 Li H, Tang J, Kang Y, *et al.* Optical properties of quasi-type-II structure in GaAs/GaAsSb/GaAs coaxial single quantum-well nanowires. Appl Phys Lett, 2018, 113: 233104
78 Rudolph D, Funk S, Döblinger M, *et al.* Spontaneous alloy composition ordering in GaAs-AlGaAs core–shell nanowires. Nano Lett, 2013, 13: 1522–1527
79 Fickenscher M, Shi T, Jackson HE, *et al.* Optical, structural, and numerical investigations of GaAs/AlGaAs core–multishell nanowire quantum well tubes. Nano Lett, 2013, 13: 1016–1022
80 Gudiksen MS, Lauhon LJ, Wang J, *et al.* Growth of nanowire superlattice structures for nanoscale photonics and electronics. Nature, 2002, 415: 617–620
81 Wu J, Ramsay A, Sanchez A, *et al.* Defect-free self-catalyzed GaAs/GaAsP nanowire quantum dots grown on silicon substrate. Nano Lett, 2016, 16: 504–511
82 Tatebayashi J, Ota Y, Ishida S, *et al.* Highly uniform, multi-stacked InGaAs/GaAs quantum dots embedded in a GaAs nanowire. Appl Phys Lett, 2014, 105: 103104
83 Tatebayashi J, Ota Y, Ishida S, *et al.* Formation and optical properties of multi-stack InGaAs quantum dots embedded in GaAs nanowires by selective metalorganic chemical vapor deposition. J Cryst Growth, 2013, 370: 299–302
84 Tatebayashi J, Ota Y, Ishida S, *et al.* Site-controlled formation of InAs/GaAs quantum-dot-in-nanowires for single photon emitters. Appl Phys Lett, 2012, 100: 263101
85 Borgström MT, Zwiller V, Müller E, *et al.* Optically bright quantum dots in single nanowires. Nano Lett, 2005, 5: 1439–1443
86 Ren D, Ahtapodov L, Nilsen JS, *et al.* Single-mode near-infrared lasing in a GaAsSb-based nanowire superlattice at room temperature. Nano Lett, 2018, 18: 2304–2310
87 Ho J, Tatebayashi J, Sergent S, *et al.* A nanowire-based plasmonic quantum dot laser. Nano Lett, 2016, 16: 2845–2850
88 Tatebayashi J, Kako S, Ho J, *et al.* Room-temperature lasing in a single nanowire with quantum dots. Nat Photon, 2015, 9: 501–505
89 Heiss M, Fontana Y, Gustafsson A, *et al.* Self-assembled quantum dots in a nanowire system for quantum photonics. Nat Mater, 2013, 12: 439–444
90 Sköld N, Wagner JB, Karlsson G, *et al.* Phase segregation in AlInP shells on GaAs nanowires. Nano Lett, 2006, 6: 2743–2747
91 Biasiol G, Gustafsson A, Leifer K, *et al.* Mechanisms of self-ordering in nonplanar epitaxy of semiconductor nanostructures. Phys Rev B, 2002, 65: 205306
92 Heinrich J, Huggenberger A, Heindel T, *et al.* Single photon emission from positioned GaAs/AlGaAs photonic nanowires. Appl Phys Lett, 2010, 96: 211117
93 Panev N, Persson AI, Sköld N, *et al.* Sharp exciton emission from single InAs quantum dots in GaAs nanowires. Appl Phys Lett, 2003, 83: 2238–2240
94 Lautenschlager P, Garriga M, Logothetidis S, *et al.* Interband critical points of GaAs and their temperature dependence. Phys Rev B, 1987, 35: 9174–9189
95 Graham AM, Corfdir P, Heiss M, *et al.* Exciton localization mechanisms in wurtzite/zinc-blende GaAs nanowires. Phys Rev B, 2013, 87: 125304
96 Jiang N, Parkinson P, Gao Q, *et al.* Long minority carrier lifetime in Au-catalyzed $GaAs/Al_xGa_{1-x}As$ core-shell nanowires. Appl Phys Lett, 2012, 101: 023111
97 Demichel O, Heiss M, Bleuse J, *et al.* Impact of surfaces on the optical properties of GaAs nanowires. Appl Phys Lett, 2010, 97: 201907
98 Skromme BJ, Sandroff CJ, Yablonovitch E, *et al.* Effects of passivating ionic films on the photoluminescence properties of GaAs. Appl Phys Lett, 1987, 51: 2022–2024
99 Sandroff CJ, Nottenburg RN, Bischoff JC, *et al.* Dramatic enhancement in the gain of a GaAs/AlGaAs heterostructure bipolar transistor by surface chemical passivation. Appl Phys Lett, 1987, 51: 33–35
100 Tajik N, Peng Z, Kuyanov P, *et al.* Sulfur passivation and contact methods for GaAs nanowire solar cells. Nanotechnology, 2011,

22: 225402
101 Chen X, Xia N, Yang Z, *et al.* Analysis of the influence and mechanism of sulfur passivation on the dark current of a single GaAs nanowire photodetector. Nanotechnology, 2018, 29: 095201
102 Tajik N, Chia ACE, LaPierre RR. Improved conductivity and long-term stability of sulfur-passivated n-GaAs nanowires. Appl Phys Lett, 2012, 100: 203122
103 Lin A, Shapiro JN, Senanayake PN, *et al.* Extracting transport parameters in GaAs nanopillars grown by selective-area epitaxy. Nanotechnology, 2012, 23: 105701
104 Yu TH, Yan L, You W, *et al.* The effect of passivation on different GaAs surfaces. Appl Phys Lett, 2013, 103: 173902
105 Alekseev PA, Dunaevskiy MS, Ulin VP, *et al.* Nitride surface passivation of GaAs nanowires: impact on surface state density. Nano Lett, 2015, 15: 63–68
106 Joyce HJ, Parkinson P, Jiang N, *et al.* Electron mobilities approaching bulk limits in "surface-free" GaAs nanowires. Nano Lett, 2014, 14: 5989–5994
107 Jiang N, Gao Q, Parkinson P, *et al.* Enhanced minority carrier lifetimes in GaAs/AlGaAs core–shell nanowires through shell growth optimization. Nano Lett, 2013, 13: 5135–5140
108 Perera S, Fickenscher MA, Jackson HE, *et al.* Nearly intrinsic exciton lifetimes in single twin-free GaAs/AlGaAs core-shell nanowire heterostructures. Appl Phys Lett, 2008, 93: 053110
109 Tateno K, Gotoh H, Watanabe Y. GaAs/AlGaAs nanowires capped with AlGaAs layers on GaAs(311)B substrates. Appl Phys Lett, 2004, 85: 1808–1810
110 Mayer B, Janker L, Rudolph D, *et al.* Continuous wave lasing from individual GaAs-AlGaAs core-shell nanowires. Appl Phys Lett, 2016, 108: 071107
111 Ho J, Tatebayashi J, Sergent S, *et al.* Low-threshold near-infrared GaAs–AlGaAs core–shell nanowire plasmon laser. ACS Photonics, 2015, 2: 165–171
112 Wei W, Liu Y, Zhang X, *et al.* Evanescent-wave pumped room-temperature single-mode GaAs/AlGaAs core-shell nanowire lasers. Appl Phys Lett, 2014, 104: 223103
113 Chang CC, Chi CY, Yao M, *et al.* Electrical and optical characterization of surface passivation in GaAs nanowires. Nano Lett, 2012, 12: 4484–4489
114 Sköld N, Karlsson LS, Larsson MW, *et al.* Growth and optical properties of strained GaAs–$Ga_xIn_{1-x}P$ core–shell nanowires. Nano Lett, 2005, 5: 1943–1947
115 Chia ACE, Tirado M, Li Y, *et al.* Electrical transport and optical model of GaAs-AlInP core-shell nanowires. J Appl Phys, 2012, 111: 094319
116 Chen S, Jansson M, Stehr JE, *et al.* Dilute nitride nanowire lasers based on a GaAs/GaNAs core/shell structure. Nano Lett, 2017, 17: 1775–1781
117 Mårtensson T, Svensson CPT, Wacaser BA, *et al.* Epitaxial III–V nanowires on silicon. Nano Lett, 2004, 4: 1987–1990
118 Chen R, Tran TTD, Ng KW, *et al.* Nanolasers grown on silicon. Nat Photon, 2011, 5: 170–175
119 Li L, Pan D, Xue Y, *et al.* Near full-composition-range high-quality $GaAs_{1-x}Sb_x$ nanowires grown by molecular-beam epitaxy. Nano Lett, 2017, 17: 622–630
120 Gerlach B, Wüsthoff J, Dzero MO, *et al.* Exciton binding energy in a quantum well. Phys Rev B, 1998, 58: 10568–10577
121 Bastard G, Mendez EE, Chang LL, *et al.* Exciton binding energy in quantum wells. Phys Rev B, 1982, 26: 1974–1979
122 Mayer B, Janker L, Loitsch B, *et al.* Monolithically integrated high-β nanowire lasers on silicon. Nano Lett, 2016, 16: 152–156
123 Hua B, Motohisa J, Ding Y, *et al.* Characterization of Fabry-Pérot microcavity modes in GaAs nanowires fabricated by selective-area metal organic vapor phase epitaxy. Appl Phys Lett, 2007, 91: 131112
124 Scofield AC, Kim SH, Shapiro JN, *et al.* Bottom-up photonic crystal lasers. Nano Lett, 2011, 11: 5387–5390
125 Gao H, Fu A, Andrews SC, *et al.* Cleaved-coupled nanowire lasers. Proc Natl Acad Sci USA, 2013, 110: 865–869
126 Wright JB, Campione S, Liu S, *et al.* Distributed feedback gallium nitride nanowire lasers. Appl Phys Lett, 2014, 104: 041107
127 Xiao Y, Meng C, Wu X, *et al.* Single mode lasing in coupled nanowires. Appl Phys Lett, 2011, 99: 023109
128 Chen R, Bakti Utama MI, Peng Z, *et al.* Excitonic properties and near-infrared coherent random lasing in vertically aligned CdSe nanowires. Adv Mater, 2011, 23: 1404–1408
129 Chen R, Ye QL, He T, *et al.* Exciton localization and optical properties improvement in nanocrystal-embedded ZnO core–shell nanowires. Nano Lett, 2013, 13: 734–739
130 Li H, Tang J, Lin F, *et al.* Improved optical property and lasing of ZnO nanowires by Ar plasma treatment. Nanoscale Res Lett, 2019, 14: 312
131 Sun H, Ren F, Ng KW, *et al.* Nanopillar lasers directly grown on silicon with heterostructure surface passivation. ACS Nano, 2014, 8: 6833–6839
132 Bermúdez-Ureña E, Tutuncuoglu G, Cuerda J, *et al.* Plasmonic waveguide-integrated nanowire laser. Nano Lett, 2017, 17: 747–754
133 Ha ST, Fu YH, Emani NK, *et al.* Directional lasing in resonant semiconductor nanoantenna arrays. Nat Nanotech, 2018, 13: 1042–1047
134 Valente J, Godde T, Zhang Y, *et al.* Light-emitting GaAs nanowires on a flexible substrate. Nano Lett, 2018, 18: 4206–4213

Acknowledgements This work was supported by the National Natural Science Foundation of China (61574022, 61674021, 61704011, 61904017, 111674038, 1404219, and 11574130), the Foundation of NANO X (No. 18JG01). Chen R acknowledges the funding support from Shenzhen Science and Technology Innovation Commission (JCYJ20180305180553701, KQJSCX20170726145748, and KQTD2015071710313656).

Author contributions This paper was written with contributions from all authors. All authors have given approval to the final version of the paper.

Conflict of interest The authors declare that they have no conflict of interest.

Haolin Li received his BE degree in electronic science and technology from Changchun University of Science and Technology in 2016. He is currently pursuing a PhD degree in electronic science and technology under the supervision of Prof. Zhipeng Wei at Changchun University of Science and Technology. His current interests include the optical properties of semiconductor nanomaterials and their applications.

Yuting Chen is currently pursuing a BE degree in optoelectronic information science and engineering under the supervision of Prof. Rui Chen at Southern University of Science and Technology. Her current interest focuses on ultrafast carrier dynamics.

Zhipeng Wei received his PhD degree in condensed matter physics from Changchun Institute of Optics, Fine Mechanics and Physics, Chinese Academy of Sciences. He is currently working at the State Key Laboratory of High Power Semiconductor Laser in Changchun University of Science and Technology. His research interests include the optoelectronic properties of low dimensional semiconductors and their applications.

Rui Chen received his PhD degree in applied physics from Nanyang Technological University, and physics from Xiamen University. He is currently working at the Department of Electrical and Electronic Engineering at Southern University of Science and Technology. His research interests include the laser spectroscopy, optical properties of materials, optical microcavity and micro/nano lasers.

GaAs基纳米线的光学性质和激射

李浩林[1,2†], 陈宇婷[2†], 魏志鹏[1*], 陈锐[2*]

摘要 工作在红外波段的砷化镓(GaAs)基纳米线激光器在集成光电子学中起着重要作用. 在过去的十几年中, 纳米线激光器领域发展迅速, 但是与工作在紫外和可见波段的材料相比, 由于GaAs基材料的特性, 近红外激光器的实现相对困难. 在本文中, 我们着重介绍了GaAs基纳米线的最新进展, 特别是GaAs纳米线的光学性质和激射特性. 详细介绍了GaAs纳米线的生长机理, 包括晶相控制和复杂结构的生长. 回顾并讨论了GaAs基纳米线的光学性质的影响因素和改进方法. 最后, 展示了GaAs基纳米线激光器的设计及其最新进展.

